Control Realization for an Interior Permanent Magnet Synchronous Motor (IPMSM) in Automotive Drive Trains

Wilhelm Peters, Tobias Huber, Joachim Böcker
Power Electronics and Electrical Drives, Paderborn University
D-33098 Paderborn, Germany
E-Mail: {peters, huber, boecker}@lea.upb.de

(The Power Point Presentation will be available after the conference.)

Abstract

The specific requirements for electrical automotive traction drives are a wide speed range, a wide constant-power operation range and high efficiency. In this paper a suitable control scheme is presented that ensures good dynamics, stability and high efficiency in the whole operation range. The focus is on the regular-sampled current control design, which requires a precise discrete-time model including the effect of a small number of sampling instants per electrical rotation. A suitable model as well as an adequate controller design is presented. The control is realized and evaluated by experimental results.

1. Introduction

Automotive electrical drives are designed to obtain high power and torque densities and thus, their behavior is considerably different from industrial drives. The main characteristics are a wide speed range, a wide constant-power operation range and a nonlinear reluctance torque due to strongly asymmetrical reluctances. Especially in pure electrical vehicles, the available energy is limited by the battery capacity and thus a high efficiency directly increases the cruising range. Therefore a suitable control scheme has to ensure a high efficiency in the whole operation range. Furthermore it has to provide stability in the entire constant power operation range particularly with a small number of sampling instants per electrical rotation at high speeds.

A suitable control scheme is presented in section 2. In this paper, the main focus is on the current controller design, which is explored in section 3. In section 4, experimental results are presented that demonstrate the adequate operation of the control, followed by the conclusion in section 5.
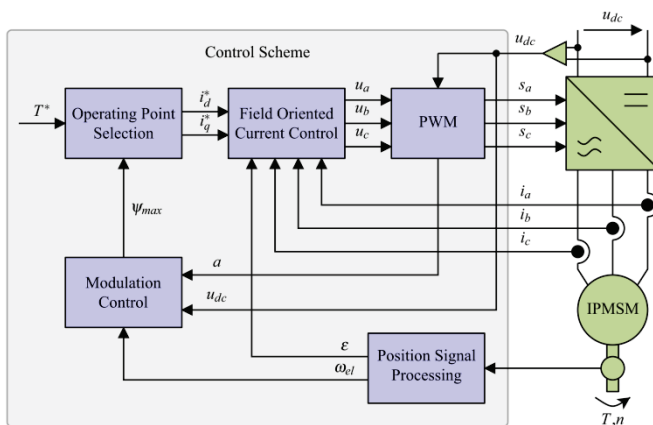
2. Control Overview

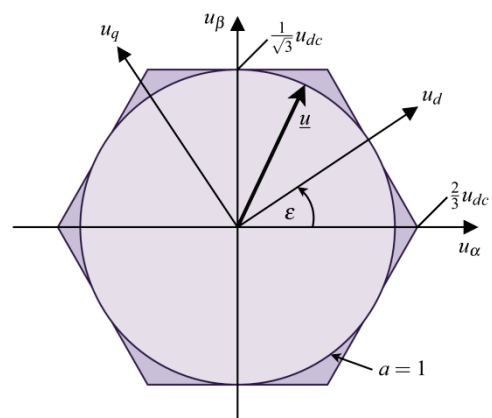Fig. 1: Control Scheme Overview

Fig. 2: Utilizable Voltage

Beside a proper inner current control loop, some auxiliary elements are required to ensure stability and high efficiency. A suitable torque control scheme including those elements is shown in Fig. 1. Especially due to the nonlinear reluctance torque, appropriate operating points have to be selected to provide the requested torque with optimal efficiency. In the constant-power operation range a modulation control (voltage control) is required to utilize the dc-bus voltage on the one hand and to keep a suitable voltage reserve to ensure the stability of the current control loop on the other hand.

2.1. Operating Point Selection

Depending on the loss characteristics of the machine, two strategies can be utilized to select appropriate operation points. If the total losses of the machine and the inverter mainly consist of losses that depend on the current magnitude, like copper losses or conduction losses, the Maximal Torque Per Current (MTPC) method provides appropriate results. The requested torque is generated with minimal current magnitude and the optimal operating points can be calculated with the method of Lagrange multipliers shown in Eq. (1). The resulting optimal reference values i_d^* and i_q^* depend on the torque reference and the maximal flux.

$$\nabla|\underline{i}(i_d, i_q)|^2 = \left[\frac{\partial|\underline{i}(i_d, i_q)|^2}{\partial i_d}, \frac{\partial|\underline{i}(i_d, i_q)|^2}{\partial i_q}\right] = \lambda\left[\frac{\partial T(i_d, i_q)}{\partial i_d}, \frac{\partial T(i_d, i_q)}{\partial i_q}\right] = \lambda\nabla T(i_d, i_q) \tag{1}$$

If there is also a remarkable amount of losses that depend on the flux magnitude, like core losses, the Maximum Efficiency (ME) method provides higher drive efficiency. The requested torque is generated with a minimum of total losses, which is typically obtained by applying a higher degree of flux weakening to the machine. That way, the overall losses are minimized by reducing the dominant core losses at the costs of higher resistive losses. The optimal reference values i_d^* and i_q^* can also be calculated with the method of Lagrange multipliers shown in Eq. (2). In contrast to the MTPC method, the resulting reference values additionally depend on the machine speed and whether it is operated in motoring or generating mode.

$$\nabla\eta(i_d, i_q) = \left[\frac{\partial\eta(i_d, i_q)}{\partial i_d}, \frac{\partial\eta(i_d, i_q)}{\partial i_q}\right] = \lambda\left[\frac{\partial T(i_d, i_q)}{\partial i_d}, \frac{\partial T(i_d, i_q)}{\partial i_q}\right] = \lambda\nabla T(i_d, i_q) \tag{2}$$

The operating point calculation can be done analytically, which requires an accurate modeling of the saturation effects for both methods and especially a precise loss modeling for the ME method. The calculation can also be performed numerically based on FEM analysis or measurements. In both cases, the results can be stored in lookup tables which are then employed in the control loop. For more details on the operating point selection and its implementation refer to [1],[2],[3] and [4].

2.2. Modulation Controller

In the constant power operation range the maximum torque at a given speed is limited by the utilizable voltage, which is limited by the hexagon shown in Fig. 2 [5]. However, the operating point selection has to ensure that the voltage vector $\underline{u}$ remains in the hexagon's inner circle during steady state operation to obtain sinusoidal voltage and current waveforms. If this objective is to be achieved in terms of an open loop control strategy, a large safety margin has to be provided. The reason lies in a number of model uncertainties such as the temperature dependency of the permanent magnets or resistive voltage drops which are neglected in the operating point selection lookup tables. Another approach is the employment of a modulation controller which is used to compensate the mentioned uncertainties [1],[6].

$$a = |\underline{u}_{\alpha\beta}|\frac{\sqrt{3}}{u_{dc}} = \sqrt{(u_\alpha^2 + u_\beta^2)}\frac{\sqrt{3}}{u_{dc}} \tag{3}$$

The corresponding modulation rate a is defined according to Eq. (3). The modulation rate is $a = 1$ when the voltage vector $\underline{u}$ rotates on the boundary of the inner circle. If the current controller output is limited to the boundary of the hexagon and the outer modulation control loop maintains a suitable dynamic distance to the inner current control loop the modulation reference can be set to $a \approx 1$ using the hexagon edges as voltage reserve for the current control loop, as will be shown in section 4.

3. Current Controller Design

The field-oriented current control loop is realized in the rotating reference frame comprising two PI-controllers for the current components i_d and i_q and a decoupling strategy. To determine the controller gains and to design an appropriate decoupling strategy a suitable motor model is required. The derivation of the motor model will be presented in section 3.1, the controller design in section 3.2.

3.1. Discrete-Time IPMSM-Modell

In the process of deriving a suitable discrete-time motor model the approximation of the flux derivative using the difference of sampled flux values is crucial. Since the motor is modeled in a rotating

reference frame, the sampled flux values used to calculate the flux difference correspond to different motor position values. Apart from the utilization of a higher order discretization method, the model accuracy can be remarkably improved by taking the alternation of the motor position during the sampling period into account [8]. Therefore, the discretization is carried out in the stationary reference frame here using the first order Euler-method and the resulting discrete-time model is transformed into the rotating reference frame [6].
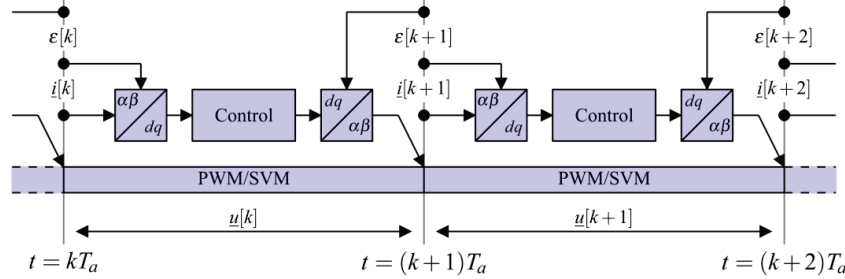

Fig. 3: Timing in Regular-Sampled Control

The current control is typically synchronized with the pulse width modulation, which is known as regular sampling. Thus, the current ripple, which is introduced by the switching of the inverter, is suppressed in the acquired data [7]. The timing of the regular sampling approach is shown in Fig. 3. Note, that the current $\underline{i}[k]$ and the rotor position $\varepsilon[k]$ are sampled values at the time instants $t = kT_a$ while the voltage $\underline{u}[k]$ is the averaged applied voltage in the sampling interval $t = [kT_a \dots (k + 1)T_a]$.

The motor model is derived from the flux differential equation in the stationary reference frame Eq. (4), which yields the flux difference equation Eq. (5) applying the first order Euler-method.

$$\frac{d\underline{\psi}_{\alpha\beta}(t)}{dt} = \underline{u}_{\alpha\beta}(t) - R\underline{i}_{\alpha\beta}(t) \tag{4}$$

$$\underline{\psi}_{\alpha\beta}[k + 1] - \underline{\psi}_{\alpha\beta}[k] = T_a\big(\underline{u}_{\alpha\beta}[k] - R\underline{i}_{\alpha\beta}[k]\big) \tag{5}$$

Applying the park transform given in Eq. (6) and (7) to Eq. (5), Eq. (8) is obtained.

$$\underline{x}_{\alpha\beta}[k] = \underline{Q}(\varepsilon[k])\underline{x}_{dq}[k] \tag{6}$$

$$\underline{x}_{\alpha\beta}[k + 1] = \underline{Q}(\varepsilon[k + 1])\underline{x}_{dq}[k + 1] \tag{7}$$

$$\underline{Q}(\varepsilon[k + 1])\underline{\psi}_{dq}[k + 1] - \underline{Q}(\varepsilon[k])\underline{\psi}_{dq}[k] = T_a\underline{Q}(\varepsilon[k])\big(\underline{u}_{dq}[k] - R\underline{i}_{dq}[k]\big) \tag{8}$$

Since the park transform does not affect the amplitude but the angle of the transformed quantity, Eq. (9) is valid. Thus Eq. (10) is obtained by left multiplication of Eq. (8) with $\underline{Q}(-\varepsilon[k + 1])$.

$$\underline{Q}(-\varepsilon[k + 1])\underline{Q}(\varepsilon[k]) = \underline{Q}(\varepsilon[k] - \varepsilon[k + 1]) = \underline{Q}(\Delta\varepsilon[k]) \tag{9}$$

$$\underline{\psi}_{dq}[k + 1] - \underline{Q}(\Delta\varepsilon[k])\underline{\psi}_{dq}[k] = T_a\underline{Q}(\Delta\varepsilon[k])\big(\underline{u}_{dq}[k] - R\underline{i}_{dq}[k]\big) \tag{10}$$

Since $\Delta\varepsilon[k]$ can be neglected at low speeds and the resistive voltage drops can be neglected at high speeds due to the high induced voltage, the effect of $\underline{Q}(\Delta\varepsilon[k])$ on the resistive voltage drops can be neglected completely. Moreover, by subtracting $\underline{\psi}_{dq}[k]$ from Eq. (10), Eq. (11) is gained.

$$\underline{\psi}_{dq}[k + 1] - \underline{\psi}_{dq}[k] = -T_aR\underline{i}_{dq}[k] + T_a\underline{Q}(\Delta\varepsilon[k])\underline{u}_{dq}[k] + \underline{Q}(\Delta\varepsilon[k])\underline{\psi}_{dq}[k] - \underline{\psi}_{dq}[k] \tag{11}$$

If the flux difference $\underline{\psi}_{dq}[k + 1] - \underline{\psi}_{dq}[k]$ is now given in Terms of the linear flux equation Eq. (12) the time-discrete model given in Eq. (13) is obtained.

$$\underline{\psi}_{dq}[k + 1] - \underline{\psi}_{dq}[k] = \begin{bmatrix} L_d & 0 \\ 0 & L_q \end{bmatrix}\big(\underline{i}_{dq}[k + 1] - \underline{i}_{dq}[k]\big) = \underline{L}_{dq}\big(\underline{i}_{dq}[k + 1] - \underline{i}_{dq}[k]\big) \tag{12}$$

$$\underbrace{\underline{i}_{dq}[k + 1] = \underline{i}_{dq}[k] - \underline{L}_{dq}^{-1}T_aR\underline{i}_{dq}[k]}_{Discrete-Time\ PT1} + \underline{L}_{dq}^{-1}T_a\left(\underbrace{\underline{Q}(\Delta\varepsilon[k])\underline{u}_{dq}[k]}_{Input\ Voltage} - \underbrace{\frac{1}{T_a}\big(\underline{\psi}_{dq}[k] - \underline{Q}(\Delta\varepsilon[k])\underline{\psi}_{dq}[k]\big)}_{Induced\ Voltage} \right) \tag{13}$$

The block diagram of the motor model is shown in Fig. 4. Assuming that $\underline{L}_{dq}$ is a diagonal matrix, the model consists of two independent PT1-elements that are coupled by the induced voltage on the one hand and the rotation of the input voltages on the other hand. Note that the induced voltage is

accurately described using the flux vector ψ_{dq} including saturation effects, but the dynamics of the PT1-elements are approximated using the constant inductances in $\underline{L}_{dq}$. Due to the rotation of the input voltage by $Q(\Delta\varepsilon[k])$, the time-discrete model properly describes the behavior of the motor in the whole speed range. Keep in mind that due to the demand for a wide speed range, the electrical frequency of automotive electrical drives reaches values of up to 1 kHz at a typical converter switching frequency of 10 kHz, which results in a small number of sampling instants per electrical period. As will be demonstrated in section 4, the controller, which is designed based on the presented discrete-time model, shows stable operation even with 10 sampling instants per electrical rotation.
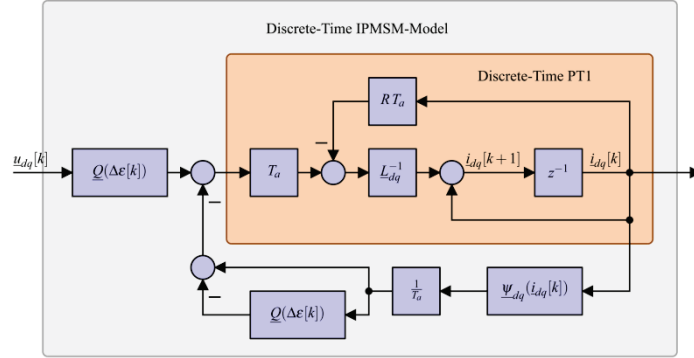

Fig. 4: Discrete-Time IPMSM Model
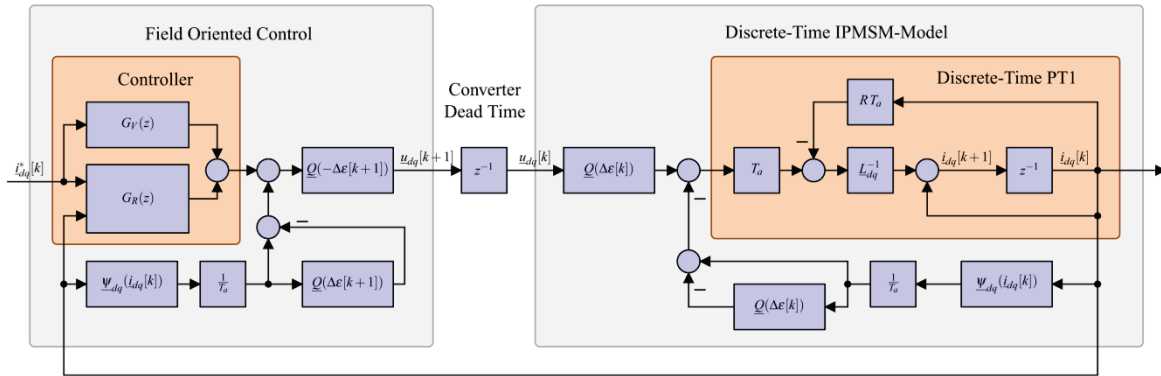
3.2. Control Structure

Fig. 5: Field Oriented Control with Decoupling

Based on the motor model presented in section 3.1, a suitable current control structure is presented in Fig. 5. The induced voltages are added to the controller output and the resulting sum is rotated by $Q(-\Delta\varepsilon[k+1])$. The function $\psi_{dq}(\underline{i}_{dq}[k])$ can be realized using lookup tables that are gained by FEM-analysis or measurements including saturation effects. That way, the plant's PT1-elements are decoupled and two independent controllers can be designed. As PI-controllers are known to be robust to parameter variations (such as saturation) if the gains are accurately adjusted, this control structure is chosen in consequence. The two employed PI-controllers in $G_R(z)$ can be tuned via their typical gains for the proportional and integral paths (K_{pd}, K_{pq}, K_{id} and K_{iq}) and moreover the reference response can be adjusted via the gains of the additional reference feed-forward paths in $G_V(z)$ (K_{vd} and K_{vq}).

$$G_{Wd}(z) = \frac{G_{Vd}(z)G_{Sd}(z) + G_{Rd}(z)G_{Sd}(z)}{1 + G_{Rd}(z)G_{Sd}(z)} \quad G_{Wq}(z) = \frac{G_{Vq}(z)G_{Sq}(z) + G_{Rq}(z)G_{Sq}(z)}{1 + G_{Rq}(z)G_{Sq}(z)} \quad (14)$$

$$G_{Wd}(z) = K_{Wd} \frac{z - \beta_d}{(z - \alpha_{d1})(z - \alpha_{d2})} \quad G_{Wq}(z) = K_{Wq} \frac{z - \beta_q}{(z - \alpha_{q1})(z - \alpha_{q2})} \quad (15)$$

If the converter dead time is neglected the reference transfer functions for the current components i_d and i_q in Eq. (14) are obtained. Both transfer functions can also be represented in terms of poles and zeros according to Eq. (15). They both consist of two poles and one zero, respectively, and are identical except for the different inductance values L_d and L_q. The controller parameters can be found

using the pole placement method. The poles of both control loops can be placed by choosing the PI-controller parameters, the zeros by choosing the feed forward gains.
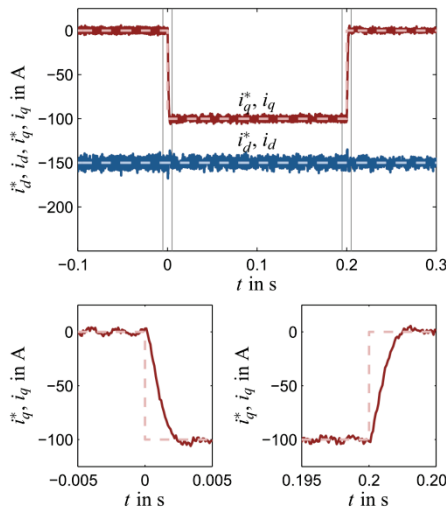
4. Experimental Results

Fig. 6: Current Step 0 A to -100 A at 6000 rpm
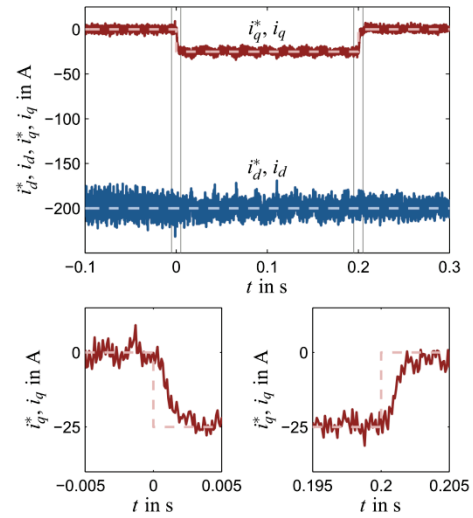

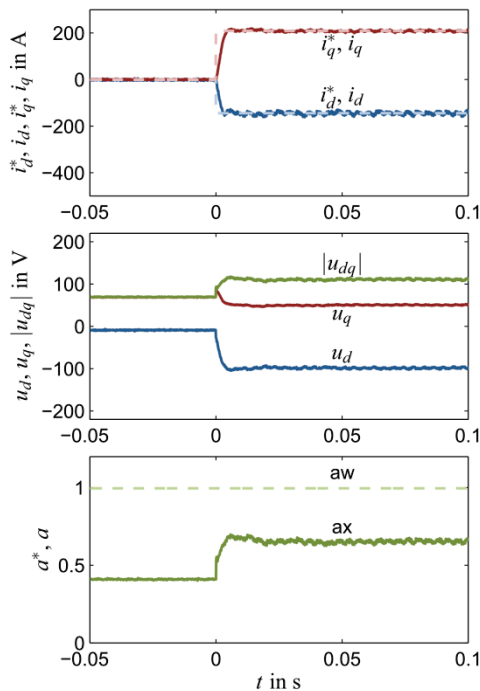Fig. 7: Current Step 0 A to -25 A at 12000 rpm
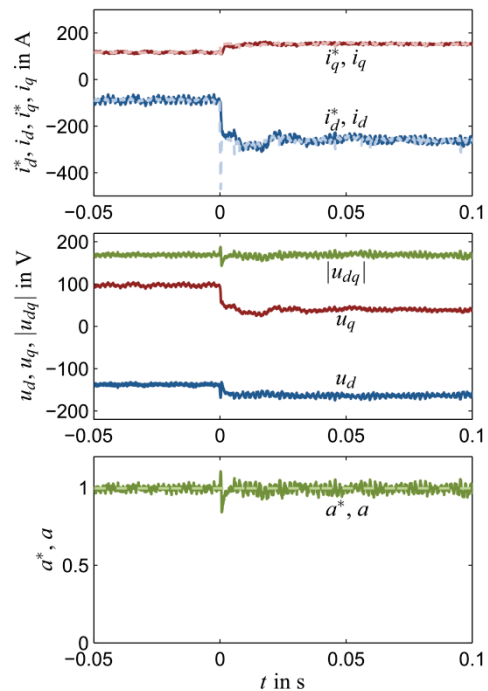

Fig. 8: Torque Step 0 Nm to 100 Nm at 3000 rpm

Fig. 9: Torque Step 50 Nm to 100 Nm at 9000 rpm

The control has been implemented on a rapid-prototyping-system according to Fig. 1 with the inner current control loop according to Fig. 5. To demonstrate the performance of the current controller, reference values have been applied manually. The corresponding step responses are shown in Fig. 6 and Fig. 7. Here reference steps have been applied to the current component i_q while keeping the current component i_d constant. The measurements demonstrate the dynamic behavior of the current controller. It becomes obvious that the decoupling is working accurately as no disturbance is seen on the current component i_d.

In Fig. 8 and Fig. 9 the performance of the entire control is demonstrated by torque reference steps. Based on the torque reference variation, appropriate operation points are chosen and impressed by the current controller. In Fig. 8 the required voltage is below the voltage limit and hence the modulation controller remains inactive. In Fig. 9, the control is operating in the constant-power operation range and the modulation controller maintains the modulation ratio a at a nominal value of $a^* = 1$. At the time instant when the current controller reacts to the reference value variation, the modulation rate increases rapidly. In consequence, the modulation controller induces the operation point selection towards a higher degree of field-weakening via a significant i_d reference rise. However, as the actual current i_d increases and the modulation ratio decreases, the field weakening current reference i_d^* also returns to lower amplitudes again. The control now operates at the nominal modulation ratio of $a^* = 1$ using the hexagon edges as voltage reserve for the current control loop, as mentioned in section 2.2.
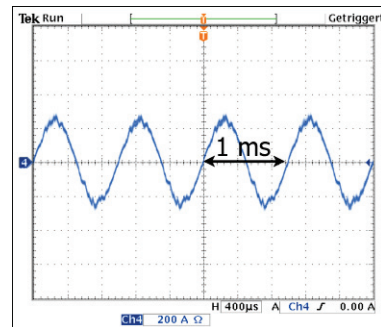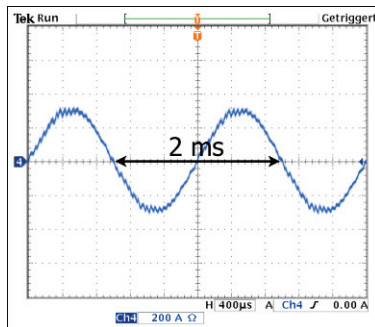

Fig. 10: Phase Current at 100 Nm and 6000 rpm   Fig. 11: Phase Current at 30 Nm and 12000 rpm

In Fig. 10 and Fig. 11 a phase current at a speed of 6000 rpm with 20 sampling instants per electrical rotation and at a speed of 12000 rpm with 10 sampling instants per electrical rotation are provided. The experimental results demonstrate the adequate and stable operation of the presented control scheme within the entire operation range.

5. Conclusion

The presented control scheme ensures good dynamics, stability and high efficiency in the whole operation range. The presented discrete-time IPMSM model is obtained by discretization of the flux differential equation in stator coordinates and transformation of the resulting flux difference equation into the rotating reference frame. The derived motor model accurately describes the behavior of the motor in the whole speed range even with a small number of sampling instants per electrical rotation at high speeds. The inner current control loop, which has been designed based on that IPMSM-model, provides an adequate performance in the entire speed range as well as good decoupling characteristics in the presence of saturation effects. The experimental results demonstrate the good dynamics and the stable operation of the presented control scheme.

Literature

[1] Böcker J., Huber T., Meyer M., Peters W., Pohlenz P., Specht A., „Control of Electric Propulsion Drives in Electric and Hybrid Vehicle / Regelung elektrischer Traktionsantriebe in Elektro- und Hybridfahrzeugen", at-Automatisierungstechnik, October 2010, Vol. 58, No. 10: 599-608.

[2] Meyer M., Böcker J.: "Optimum Control for Interior Permanent Magnet Synchronous Motors (IPMSM) in Constant Torque and Flux Weakening Range", EPE-PEMC, 2006, Portoroz

[3] Pohlenz D., Böcker J.: "Efficiency Improvement of an IPMSM using Maximum Efficiency Operating Strategy", EPE-PEMC 2010, Ohrid, Makedonien, Sept. 2010

[4] Mademlis C., Kioskeridis I., Margaris N., "Optimal efficiency control strategy for interior permanent-magnet synchronous motor drives", IEEE Transactions on Energy Conversion, Vol. 19, No. 4, 2004

[5] Quang N.P., Dittrich J.-A., „Vector Control of Three-Phase AC Machines", Springer, 2008

[6] Meyer M.: „Wirkungsgradoptimierte Regelung hoch ausgenutzter Permanentmagnet-Synchronmaschinen im Antriebsstrang von Automobilen", Dr.-Ing. Thesis, Paderborn University, 2010

[7] Peters W., Schulz B., Mathapati S., Böcker J.: „Regular-sampled Current Measurement in AC-drives using Delta-Sigma-Modulators", EPE, 2009, Barcelona

[8] Böcker J., "Discrete-Time Model of an Induction Motor", ETEP Vol. 1, No. 2, March/April 1991